Wind and Structures, *Vol. 27, No. 6 (2018) 000-000*
DOI: https://doi.org/10.12989/was.2018.27.6.000

Wind tunnel study of plume dispersion with varying source emission configurations

Adrián R. Wittwer*[1], Acir M. Loredo-Souza[2a], Edith B. Camaño Schettini[3b] and Hugo G. Castro[4c]

[1]*Laboratorio de Aerodinámica, Facultad de Ingeniería, Universidad Nacional del Nordeste (UNNE), Postal Code 3500, Resistencia, Chaco, Argentina*
[2]*Laboratório de Aerodinâmica das Construções, Universidade Federal do Rio Grande do Sul, PO Box 15035, PC 91501-970, Porto Alegre, Rio Grande do Sul, Brazil*
[3]*Instituto de Pesquisas Hidráulicas, Universidade Federal do Rio Grande do Sul, PC 91501-970, Porto Alegre, Rio Grande do Sul, Brazil*
[4]*Instituto de Modelado e Innovación Tecnológica, Consejo Nacional de Investigaciones Científicas y Técnicas (CONICET), Universidad Nacional del Nordeste, PC 3500, Resistencia, Chaco, Argentina*

(Received April 21, 2017, Revised June 29, 2018, Accepted August 1, 2018)

Abstract. The concentration fields in the proximities of a local gas emission source are experimentally analyzed in several combinations of wind incidences and source emissions. These conditions are determined by the plume buoyancy, emission velocity and incident flow wind speed. Concentration measurements are performed by an aspirating probe in a boundary layer wind tunnel. The analysis included the mean concentration values and the intensity of concentration fluctuations in a neutral atmospheric boundary layer flow. Different configurations are tested: an isolated stack in a homogeneous terrain and a stack with a bluff body in close proximity, located windward and leeward from the emission source. The experimental mean concentration values are contrasted with Gaussian profiles and the dilution factor is analyzed with respect to the empirical curves of the minimum dilution. Finally, a study on the plume intermittency is performed in a cross-sectional plane near the emission source. It is possible to highlight the following observations: a) plume vertical asymmetry in the case of an isolated emission source, b) significant differences in the dispersion process related to the relative location of the emission source and bluff body effects, and c) different probabilistic behavior of the concentration fluctuation data in a cross-sectional measurement plane inside the plume.

Keywords: plume dispersion; wind tunnel modeling; tracer gas; probabilistic analysis

1. Introduction

The study of dispersion and pollutant concentration levels discharged in the atmosphere has become a fundamental issue due to its recognized impact on the environment. Through the years, different approaches were used in order to study this subject in a more accurate way. Field measurements are the less common methodology since these studies are, generally, extremely expensive and rather impractical. The other two main procedures are physical modeling in wind tunnels and numerical simulation with Computational Fluid Dynamics (CFD).

Nowadays, numerous computational works related with dispersion phenomena are being developed. Usually these studies must be validated with experimental results. The high costs of field experimentation lead to laboratory reduced model studies. In this context, the boundary layer wind tunnel becomes an important tool, where the main characteristics of the atmospheric boundary layer (ABL) and of the dispersion processes need to be reproduced.

To reproduce dispersion phenomena in wind tunnels, besides the requirements of simulation of the atmospheric boundary layer, similarity requirements are established to the modeling of the plume emission behavior. These requirements, according to Isyumov and Tanaka (1980), may be summarized in the following way: source geometric similitude, Froude number similarity, density and velocity ratio similarities as well as similarity of the source Reynolds number.

The practical difficulties related to the exact simulation of the emission process make approximate solutions an acceptable alternative. Cermak and Takeda (1985) proposed that besides geometric similarity, equality of Richardson number and boundary condition similarity, it is important to consider other criteria for similarity of source characteristics. These additional conditions are: equality of the relationship between the emission velocity and the local wind velocity, and the equality of densimetric Froude number. Furthermore, the similarity criteria may be modified according to the region of interest, which may range from a region closest to the source, in which the own chimney structure and the discharge cause modifications into the flow field, to a further zone, where these effects are not observed.

*Corresponding author, Dr.
E-mail: a_wittwer@yahoo.es
[a] Ph.D.
E-mail: acir@ufrgs.br
[b] Dr.
E-mail: bcamano@iph.ufrgs.br
[c] Dr.
E-mail: guillermo.castro@conicet.gov.ar

 ISSN: 1226-6116 (Print), 1598-6225 (Online)

It is well known that factors like height and location of stack emissions affect the pollutant dispersion. But the characteristics of pollutants mixing is also greatly modified if a stack is surrounded by buildings or structures. Thompson (1993) conducted a wind tunnel study in order to determine pollutant concentrations at ground level and around buildings which demonstrated the high dependency between the stack placement and the obstacles around it. Recently, Perry *et al*. (2016) also studied this phenomena using a wind tunnel but examining the influence of elongated rectangular buildings on the near-field dispersion. The study reported that for these type of buildings wind direction has a strong impact on ground-level concentration patterns.

There is also a great amount of work done in the area of computational wind engineering (CWE) (Quinn *et al*. 2001, Fothergill *et al*. 2002, Kim et al. 2006, Lateb *et al*. 2011, Gousseau *et al*. 2011, Gousseau *et al*. 2012, Vervecken *et al*. 2013, Yu and Thè 2016). Studies using CFD allowed a great advance in the characterization of pollutant emissions and gas dispersion but there is still a high demand for experimental data to more thoroughly characterize these phenomena.

In this work the dispersion process of an emission plume is studied through a reduced scale model in a boundary layer wind tunnel. The source model represents a buoyant plume (gas emission) that disperses into a neutrally stable turbulent boundary layer. Several conditions are considered, determined by the degree of the plume buoyancy, discharge emission velocity and approaching flow velocity, as well as two different configurations of the surroundings. The modification on the surroundings is represented by a simple building model located in two different positions, windward and leeward of the emission source.

In wind tunnel dispersion modeling, according to Robins *et al*. (2001), different aspects must be studied to improve the understanding of dispersion processes in the atmosphere and to solve specific problems. The areas included in this paper are: basic dispersion processes near the emission, nearby building effects and concentration fluctuations. The following Section provides a description of the experimental tests performed in the wind tunnel. The results and discussions are presented in Section 3 and conclusions are drawn in Section 4.

2. Experimental design

2.1 Wind tunnel and model arrangements

In this work, the tests were performed at the "Prof. Joaquim Blessmann" wind tunnel of the Universidade Federal do Rio Grande do Sul (UFRGS), Brasil. This boundary layer wind tunnel has a closed return configuration with a test section 1.30 m wide, 0.90 high and 9.32 m long. A neutrally stable boundary layer is obtained by using rows of roughness elements placed on the wind tunnel floor and spires as vortex generator devices (Blessmann 1982).

To perform atmospheric diffusion studies it is usual to consider full scale wind speeds in the range of 5 to 20 m/s (Isyumov and Tanaka 1980). Thus, in order to fulfill the Froude number similarity given by

$$\left(\frac{z_{ref}\,g}{U_{ref}^2}\right)_m = \left(\frac{z_{ref}\,g}{U_{ref}^2}\right)_p \qquad (1)$$

the wind tunnel modeling must be performed at low free-stream mean velocities. In Eq.(1), g is the acceleration of gravity and U_{ref} indicates the mean velocity at the reference height z_{ref}. Also, subscripts m and p represent model and full scale quantities, respectively.

In Fig. 1 the non-dimensional profiles obtained with U_{ref1} = 0.85 m/s and U_{ref2} = 1.91 m/s are compared with the highest mean velocity achievable in the wind tunnel ($U_{ref}^{max} \approx 35$ m/s). The mean velocity profile given by the power-law expression,

$$\frac{U(z)}{U_{ref}^{max}} = \left(\frac{z}{z_{ref}}\right)^{\alpha} \qquad (2)$$

is also shown in Fig. 1. In Eq. (2) the power-law exponent α is equal to 0.23 and z_{ref} = 450 mm is the reference height, being z the height above the wind tunnel floor. Also, turbulence intensities measured in correspondence to U_{ref1}, U_{ref2} and U_{ref}^{max} are shown in Fig. 1.

Turbulence intensity values corresponding to U_{ref2} are slightly higher than those obtained at high velocity, which a behavior commonly observed at low velocities. For measurements at velocity U_{ref1} it is possible to observe even larger deviations in comparison with U_{ref}^{max} and U_{ref2} cases that can be attributed to the extremely low velocity. It is worth noting that with these velocity magnitudes the relative errors affecting the anemometric probes are larger than for measurements at high velocities. This kind of behavior were also observed in similar wind tunnel tests using three-dimensional Laser Doppler Velocimetry (Yassin *et al.* 2005). Furthermore, additional measurements were obtained in order to ensure that the simulated boundary layer was fully developed.

The emission source model is a circular tube of diameter D_0 equal to 20 mm and variable height H, Fig. 2. Pure helium (*He*) as well as an air-helium (*He-Air*) mixture were used as tracer gases. In addition to U_{ref1} and U_{ref2}, another velocity, U_{ref3} = 3.04 m/s, was used in order to allow the modification of the plume characteristic parameters. Furthermore, three cases were analyzed: the isolated stack in a homogeneous terrain (configuration *I*, Fig. 2) and the stack with a single prismatic building in its surroundings, located at windward and leeward of the emission source (configurations *II* and *III*, respectively, Fig. 3). In Figs. 2 and 3, x indicates the distance between the emission source and the measurement plane.

In configuration *I*, the height of the chimney is H = 250 mm. For configurations *II* and *III*, the building height B is 270 mm, while H varies from 250 to 270 mm according to the test performed. The separation between the chimney and the building model in both cases is equal to 80 mm.

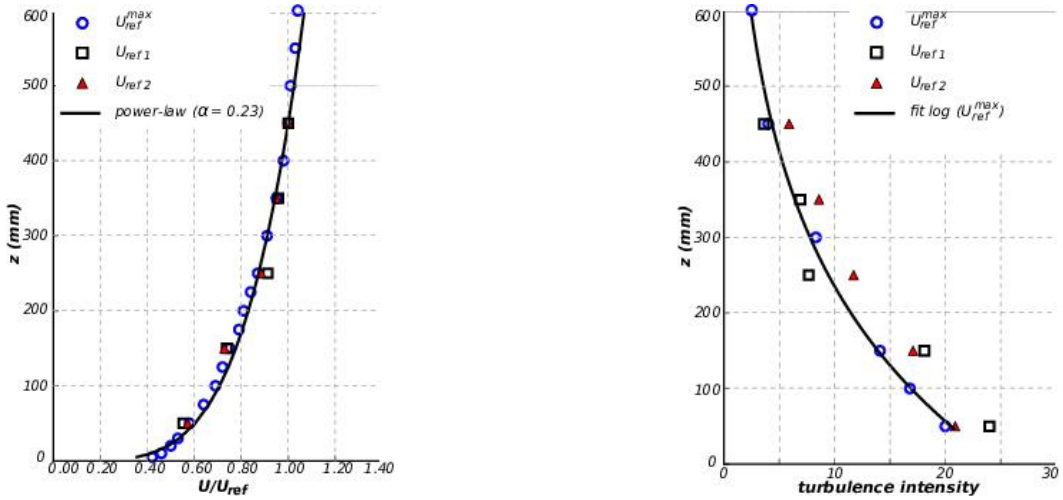

(a) Wind speed profile (b) Turbulence intensity profile

Fig. 1 Non-dimensional mean wind velocity (a) and local turbulence intensity (b) profiles. For the local turbulence intensities, the solid line represents a logarithmic function fitted to the values corresponding to U_{ref}^{max}

2.2 Plume modeling

The plume characteristic conditions (from *a* to *h*) are determined by the non-dimensional parameters indicated in Table 1. In this work, three scaling parameters were taken into account (Cermak and Takeda 1985):

1. Ratio between the emission velocity (w0) and the approaching low velocity(U0), known as plume velocity ratio

$$\frac{w_0}{U_0} = constant \tag{3}$$

2. Plume momentum,

$$\frac{\rho_0 w_0^2}{\rho_a U_0^2} = constant \tag{4}$$

where ρ_0 and ρ_a are the stack exhaust gas density and the ambient air density, respectively. Conditions (*d*) and (*h*) are referred to emissions of mixtures helium-air with density values of 0.462 and 0.325 kg/m3, respectively.

3. Buoyancy parameter,

$$\frac{(\rho_0 - \rho_0) g w_0 D_0}{\rho_a U_0^3} = constant \tag{5}$$

Maintenance of this dimensionless parameters enables a correct representation of the plume behavior when it is released from an elevated point source.

Generally, atmospheric Reynolds number cannot be reproduced in a wind tunnel test. Nevertheless, maintenance of Reynolds number independence, according to Robins *et al*. (2001), can be achieved provided that the roughness Reynolds number is larger than 1, that is

$$Re(z_0) = u^* z_0 / \nu \geq 1 \tag{6}$$

where u^* is the friction velocity, z_0 is the roughness length and ν the kinematic viscosity. In this work, the lower limit is established by the lower reference velocity, U_{ref1} = 0.85 m/s, resulting in a value of $Re(z_0)$ equal to 3.9. In Eq. 6, the parameters u^* and z_0 were obtained using the methodology proposed by Liu *et al.* (2003). In this method, the turbulent intensity profile of the turbulent surface layer is used to calculate z_0, replacing it then into the mean wind speed profile in order to obtain u^*. This procedure also requires to change the wind tunnel measured data with the field data with a geometric scale factor of 1:300 (Blessmann1982, Loredo-Souza *et al.* 2004).

For configurations *II* and *III*, where a prismatic model is immersed in the flow, the characteristic Reynolds number $Re_H = U_H H/\nu$, verify the condition $Re_H > 3300$ (White and Stein 1990) where H is the characteristic height and U_H is the velocity at height H.

2.3 Measurement techniques

The concentration field of the plume dispersion process was evaluated leeward from the emission source, at a variable distance *x*. The measurements were performed by a hot-wire anemometer with an aspirating probe (Harion *et al.* 1996). This probe is composed by a hot wire and a 0.3 mm internal diameter ceramic tube, connected to a vacuum pump. The hot-wire anemometer, by incorporating the aspirating probe, becomes a density measurement system and when binary gas mixtures are used the system measures instantaneous concentrations. A gas mixer was used to provide known air-helium mixtures to calibrate the probe (Camano Schettini 1996). This type of probe produces a wide useful bandwidth of frequency response and it allows the evaluation of the plume fluctuating concentration near the source in a turbulent wind. At each measurement point, a sample of one minute was taken at a sampling frequency of 1024 Hz.

Fig. 2 Isolated emission, configuration I.

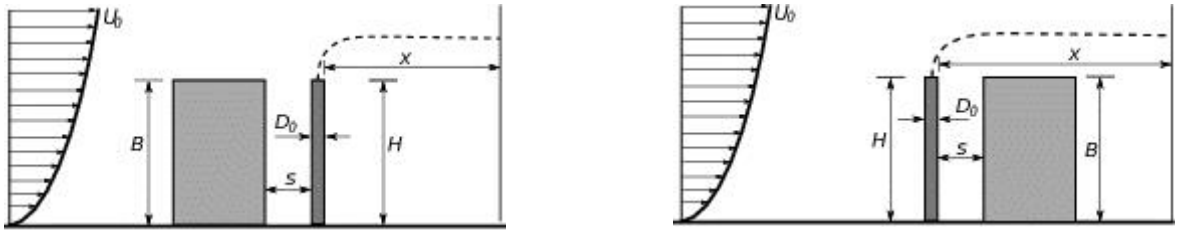

(a) Configuration *II* (b) Configuration *III*

Fig. 3 Single prismatic building model located windward (a) and leeward (b) from the emission source, respectively

Table 1 Characteristic parameters of the plume model

Condition	Emission	w_0 (m/s)	U_0 (m/s)	Dimensionless parameters		
				Eq. 3	Eq. 4	Eq. 5
(a)	*He*	0.56	0.85	0.66	0.060	-0.154
(b)	*He*	1.96	1.91	0.66	0.060	-0.031
(c)	*He*	0.95	0.85	1.11	0.171	-0.260
(d)	*He-Air*	0.75	0.85	0.88	0.278	-0.154
(e)	*He*	0.56	3.04	0.18	0.005	-0.003
(f)	*He*	0.95	3.04	0.31	0.013	-0.006
(g)	*He*	0.56	1.91	0.29	0.012	-0.014
(h)	*He-Air*	1.45	1.91	0.76	0.145	-0.031

In this work, the results obtained in the tests are presented as profiles of concentration coefficient (K) and intensity of the concentration fluctuations (I_c)

$$K = \frac{CU_H H^2}{Q_0} \tag{7}$$

$$I_c = \frac{\sigma_c}{C} \tag{8}$$

where C and σ_c are the mean concentration and the standard deviation (rms) of the concentration fluctuations, respectively; Q_0 is the total exhaust volume flow rate (m^3/s), U_H is the wind velocity at the emission source height (stack height) and z is the vertical coordinate measured from the wind tunnel floor.

3. Results

Vertical profiles of instantaneous concentrations were measured at several distances x/H from the emission source and are presented in Figs. 4 to 13. Mean concentration and corresponding rms values were obtained for each measurement point.

3.1 Configuration I

Fig. 4 presents vertical profiles of concentration coefficient K and I_c for condition (*a*) and configuration *I* (no building model), related to the positions x/H=0.33, 0.66 and 1.00. Profiles of K and I_c at positions x/H=2.00, 3.00, 3.80 for the same situation are shown in Fig. 5. Due to buoyancy effects, the profiles present asymmetries, tending to deviate the plume upwards.

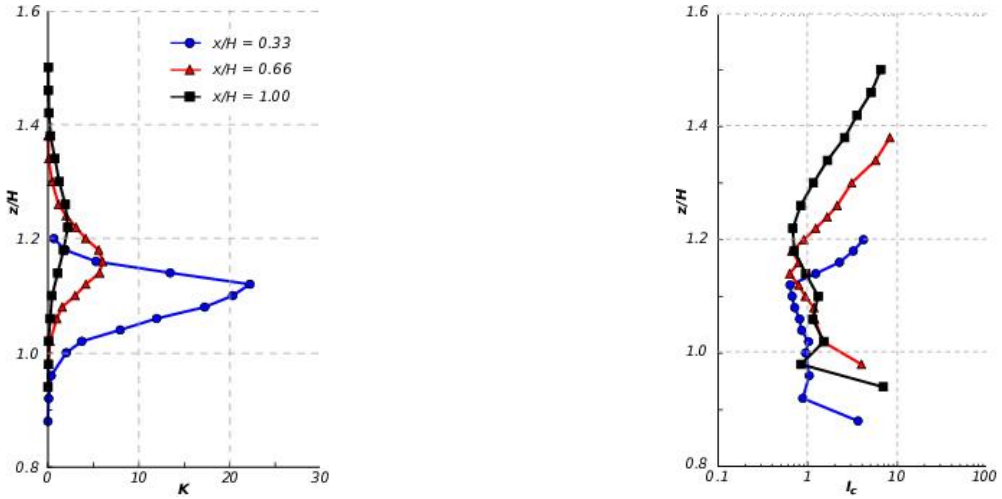

Fig. 4 Concentration profiles K and I_c, condition (*a*), configuration *I*, at x/H = 0.33, 0.66 and 1.00

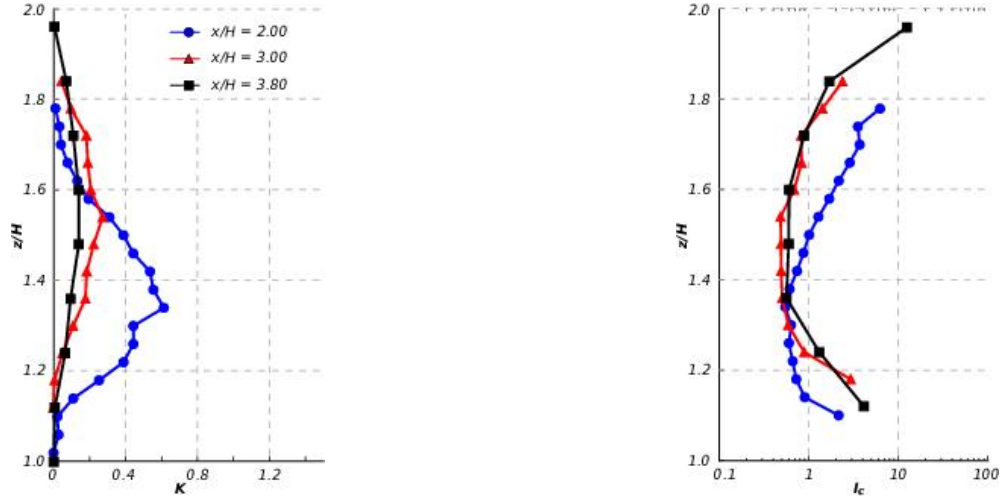

Fig. 5 Concentration profiles K and I_c, condition (*a*), configuration *I*, at x/H = 2.00, 3.00 and 3.80

Similar behavior is observed in Fig. 6, related to condition (*b*) and to the same configuration *I*, for three leeward positions x/H=0.60, 1.20, 1.80. From the comparison of these two situations is possible to infer that, even preserving emission velocity and momentum parameters, the behavior of the plume is not the same for these two cases owing to different buoyancy characteristics (see Eq. (5) and Table 1). Furthermore, it can be noted that the profiles of I_c show large irregularities at the lower region of the plume. These irregularities decrease as x/H increases and are larger for condition (*a*) where the incident flow velocity is 0.85 m/s. Nevertheless, the asymmetric behavior relative to the upper and the lower part of the plume persists.

In Fig. 7, lateral profiles for condition (*a*) at x/H=0.33 and z/H=1.12, and for condition (*b*) at x/H=0.60 and z/H=1.10 are shown. Lateral symmetry of the plume is evident in both cases.

Fig. 8 show vertical profiles of K and I_c in proximity of the emission source for configuration *I*. With a lower emission velocity w_0, is observed that the plume decline for condition (*e*) whereas for condition (*f*), the plume center coincides with the source height. All cases present an asymmetric behavior of the plume configuration, meaning that the vertical dispersion parameter σ_z has a lower value in the upper profile region with respect to the lower profile region. Maximum concentration levels and vertical displacement of the center plume show coherency with emission and wind velocity conditions. Smaller values on the upper region as well as some irregularities can also be noted in the vertical profiles of I_c for conditions (*c*) and (*d*).

Three vertical profiles in the far away region of the emission source for configuration *I* are analyzed in Fig. 9. For condition (*a*) and position x/H=2.00, inertial effects are low and the profile presents some minor irregularities. For position x/H=1.80 with conditions (*b*) and (*h*), inertial effects are greater than the previous case and the plume configuration is almost Gaussian. Different values of elevation (plume rising) Δ_z and vertical dispersion σ_z are observed in cases (*b*) and (*h*) associated to different emission momentum for each condition.

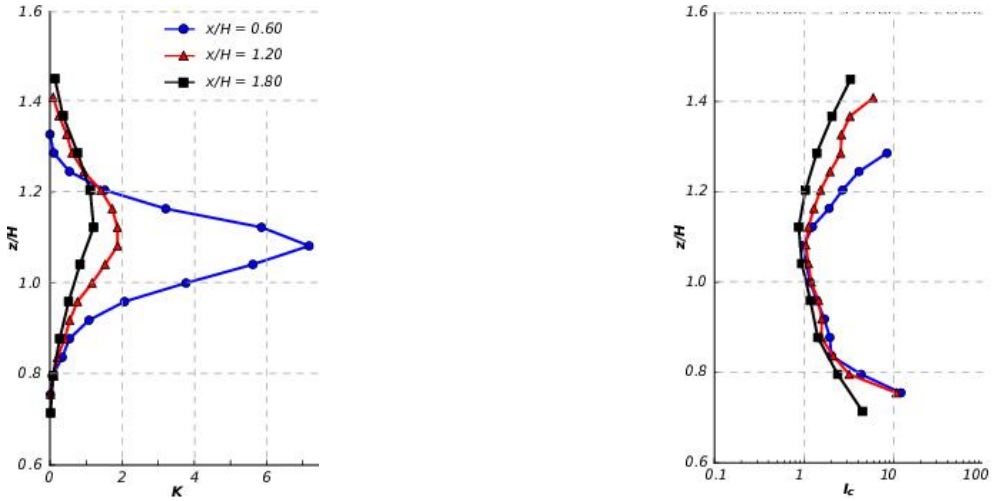

Fig. 6 Concentration profiles K and I_c, condition (b), configuration I, at x/H = 0.60, 1.20 and 1.80

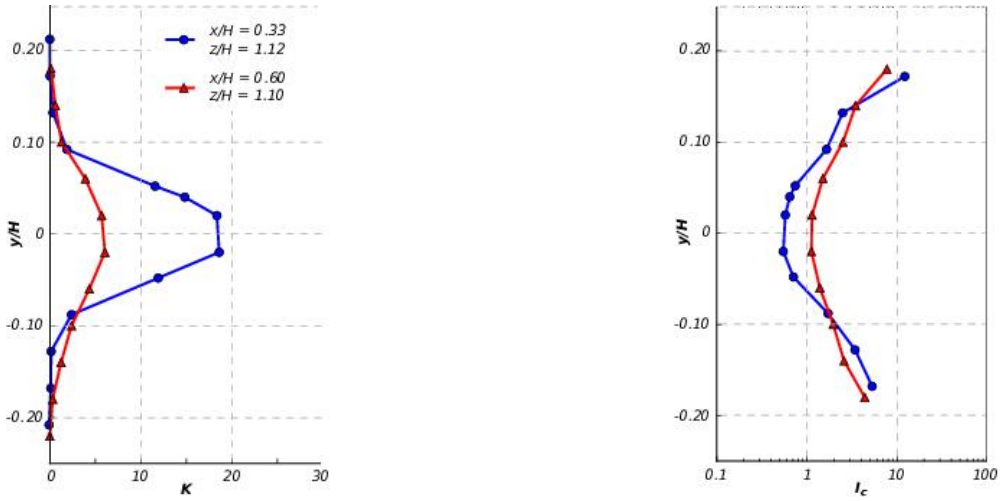

Fig. 7 Concentration lateral profiles K and I_c, configuration I, condition (a), configuration I, at x/H = 0.33, z/H = 1.12 and condition (b) at x/H = 0.60, z/H = 1.10

Small values at the upper and lower regions in the I_c profiles for condition (h) determine a practically constant value of I_c for all plume wide.

Vertical profiles measured at x/H=0.60 for configuration I and conditions (b), (g)} and (h) are compared in Fig. 10. From this figure is evident the dependency of the plume centroid location, Δ_z, on the plume buoyancy and emission momentum. Furthermore, a small variation of the plume spread can be observed. In these cases, the plume buoyancy variation is produced only by the difference of emission velocity since the incident velocity practically does not vary.

3.2 Configuration II

Fig. 11 shows vertical profiles corresponding to configuration II, for condition (a) at two positions (x/H=0.315 and 0.630) and for condition (b)} at three positions (x/H=0.315, 0.630 and 1.260). The smaller absolute values of K with respect to configuration I indicate a greater dilution effect on the concentrations caused by the flow conditions imposed by the presence of the building model. This effect is also denoted by an increase of the vertical dispersion σ_z and a non-gaussian configuration for K. In the leeward position, the level of concentration fluctuations is much lower than configuration I, where the observed I_c deviations at this position are explained as a result of the aspirating probe resolution, since the corresponding mean concentration values are very low.

3.3 Configuration III

The profiles corresponding to configuration III are presented in Fig. 12. In the cases x/H=0.540 (a1) and 1.080 (a), the stack height matches the building height and the K profiles are clearly Gaussian. For x/H=0.540 (a2), the height ratio between chimney and building is equal to 0.96 and a distortion is produced in the lower part (close to the top of the building model) in comparison with a Gaussian behavior.

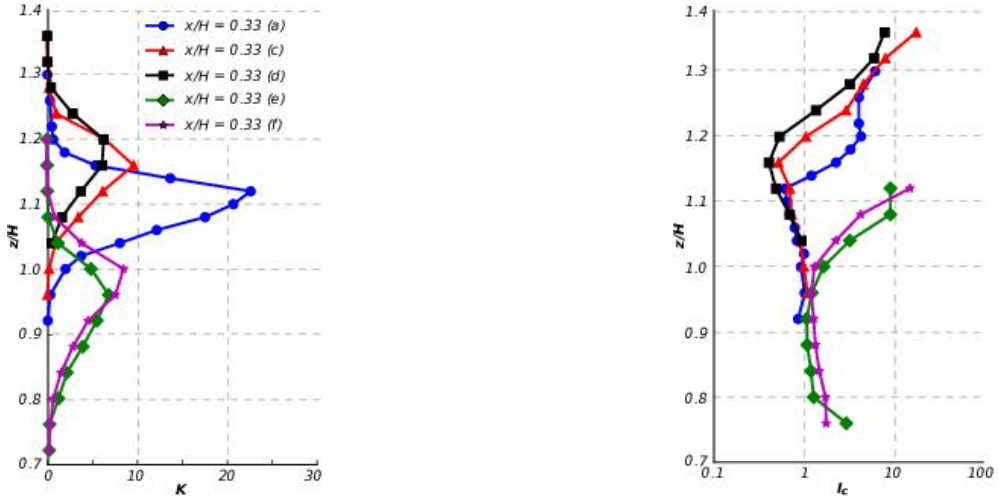

Fig. 8 Comparison of concentration profiles K and I_c, configuration *I*, for conditions (*a*), (*c*), (*d*), (*e*) and (*f*)

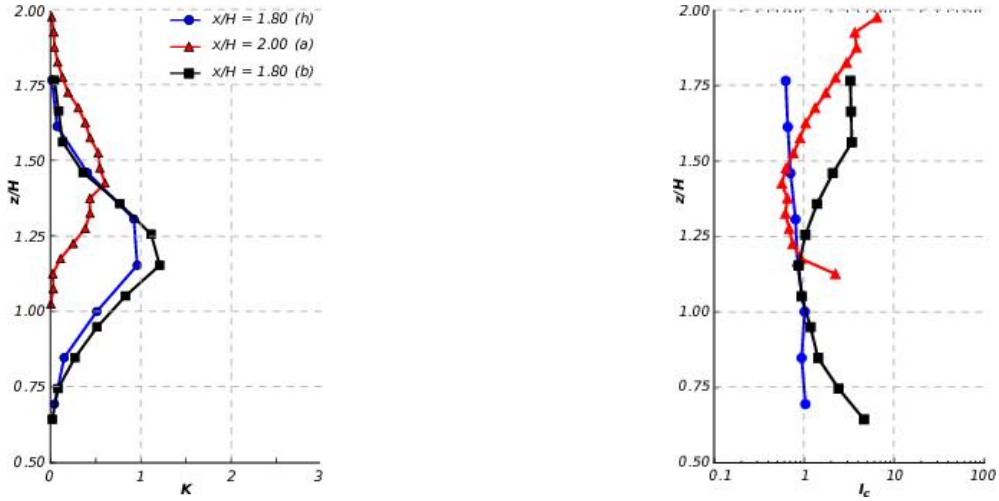

Fig. 9 Comparison of concentration profiles K and I_c, configuration *I*, for conditions (*a*) with x/H = 2.00, (*b*) and (*h*) with x/H = 1.80

These three cases correspond to condition (*a*) where inertial effects are smaller, the effective plume height ($H + \Delta_z$) increases, allowing the discharge, almost completely, of the plume from the wake region. In cases x/H=0.540 (*b*1) and (*b*2), the ratio of heights between stack and building is equal to 1.00 and 0.93, respectively. Inertial effects are larger for condition (*b*) decreasing the plume effective height and therefore increasing the concentration level in the lower part (close to the top of the model). The intensities of concentration fluctuations decay significantly in this region of the profile.

In comparing Figs. 10-12, it can be noted different behaviors of the plume for configurations *I*, *II* and *III*. It is clear that concentration levels, values of Δ_z and σ_z and vertical distribution of I_c indicate specific behavior characteristics for each situation. Fig. 13 shows the vertical profiles in proximities of the emission source, x/H=0.54, 0.60 and 0.63, for condition (*b*), where is possible to observe the effects caused by the different configurations. A higher plume elevation is observed for configuration *III* with respect to configuration *I*. Also, an appreciable increment of the vertical dispersion σ_z is obtained for configuration *II*. This effect is directly related to the location of the emission source, which is placed into the building model wake for this particular configuration.

3.4 Gaussian plume analysis

The experimental values obtained for configuration *I* were fitted to the Gaussian plume expression

$$\frac{C(z)}{C_0} = \exp\left[\frac{(z - z_C)^2}{2\sigma_z^2}\right] \tag{9}$$

which enables to determine the vertical dispersion parameter σ_z.

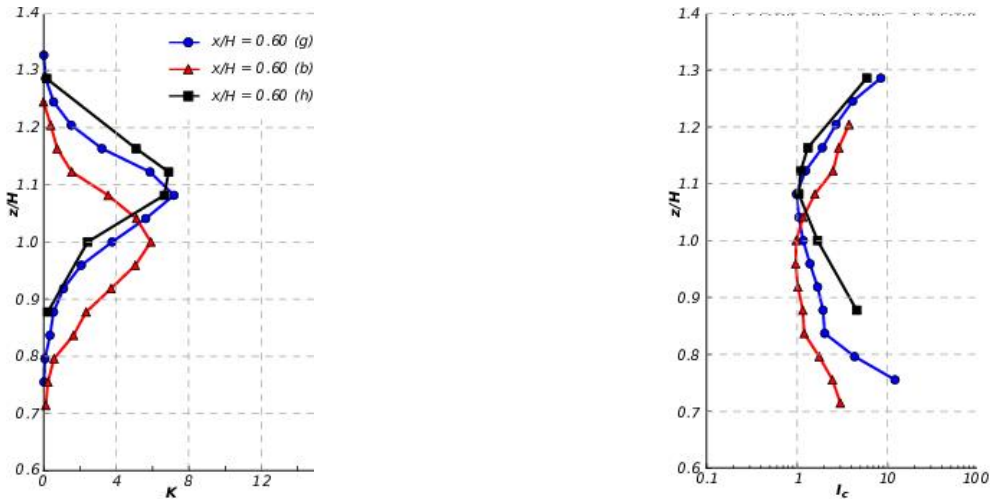

Fig. 10 Comparison of concentration profiles K and I_c, configuration I, for conditions (*b*), (*g*) and (*h*) with $x/H = 0.60$

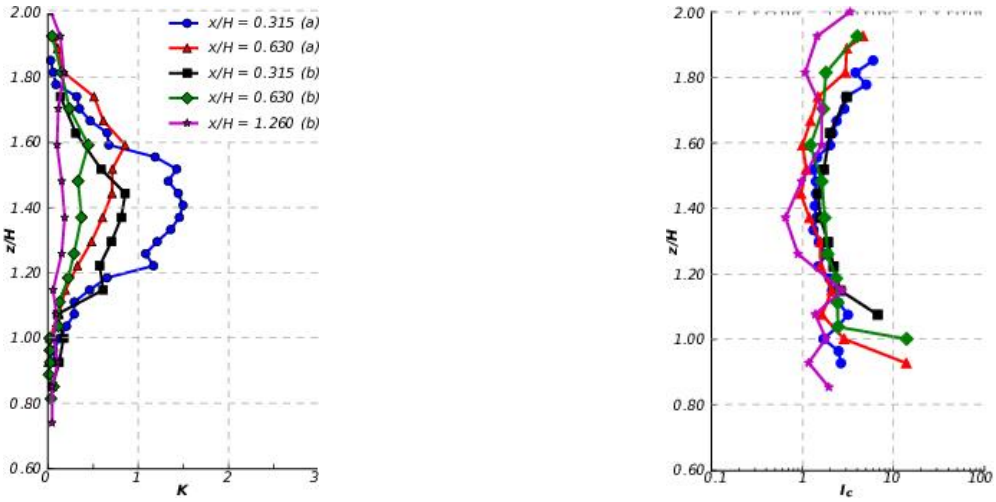

Fig. 11 Concentration profiles K and I_c, configuration II, for conditions (*a*) and (*b*)

In Eq. (9), C_0 is the maximum mean value of the concentration (plume centreline) and z_C is its position in the plume. Figs. 14 and 15 show the vertical non-dimensional concentration profiles corresponding to six leeward emission positions, considering condition (*a*) for configuration *I*. In Fig. 16, values corresponding to three positions for condition (*b*) are compared. Due to the asymmetry of profiles, the representation is made considering one value of the parameter σ_z for the upper region and another one for the lower region. The fitness of the values to the Gaussian profile is acceptable, but the quality diminishes at positions farther from the emission source.

In Fig. 17, values of the parameter σ_z are plotted against the distance x/H, for conditions (*a*) and (*b*), configuration *I*. This figure also compares the experimental values with the Briggs' expression given by Zannetti (1990) and Baechlin *et al.* (1992), for neutral atmospheric stability conditions in urban and rural areas.

3.5 Dilution analysis

The dispersion process was analyzed from the dilution factor defined by the expression $D = C_e/C_0$ at near-field from the gas emission source, being C_e the mean concentration at the emission source. Values obtained in these measurements are compared with a prediction model of the minimum dilution proposed by Chui and Wilson (1988)

$$D_{\min} = \left[D_M^{0.5} + 0.25 \left(\frac{U_0 x^2}{Q_0} \right)^{0.5} \right]^2 \tag{10}$$

where $D_M = 1 + 7M^2$, being M the exhaust momentum factor

$$M = \left(\frac{\rho_0}{\rho_a} \right)^{0.5} \frac{w_0}{U_0}. \tag{11}$$

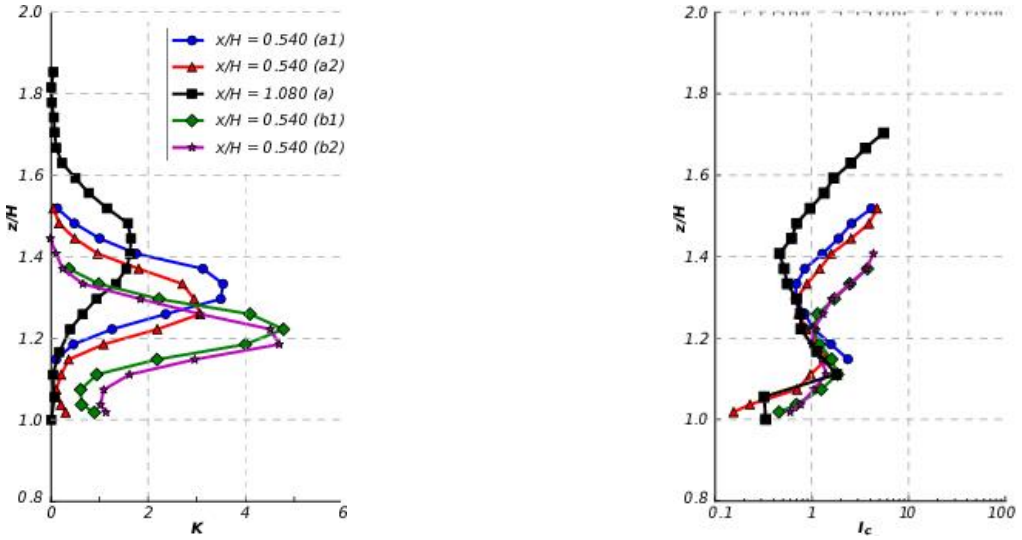

Fig. 12 Concentration profiles K and I_c, configuration *III*, condition (*a*): x/H = 0.540 and 1.080, and condition (*b*): x/H = 0.540

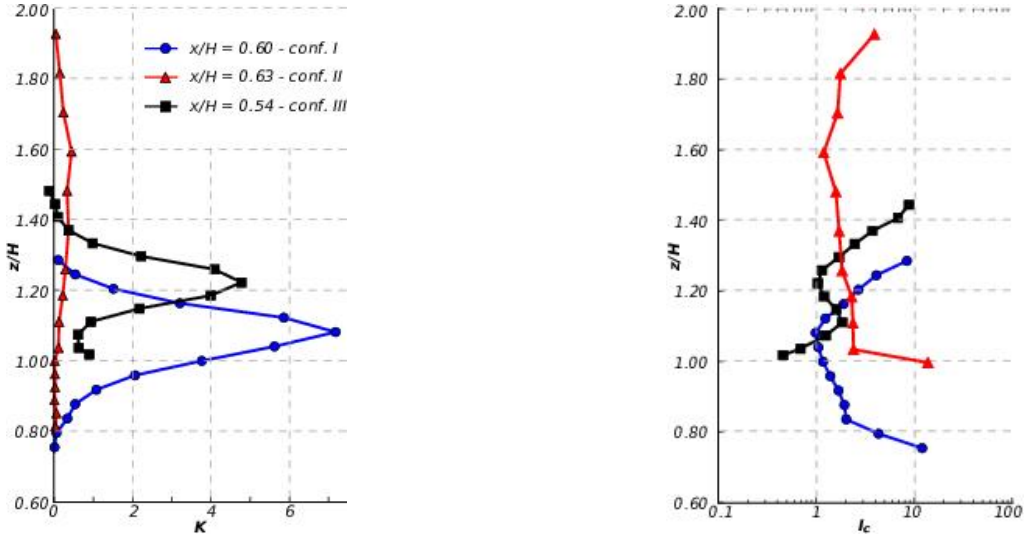

Fig. 13 Concentration profiles K and I_c, configuration *I*, *II* and *III* for condition (*b*)

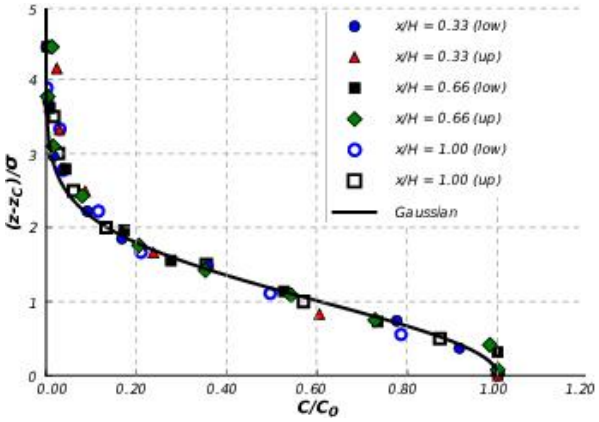

Fig. 14 Gaussian profile and mean concentration experimental values, configuration *I*, condition (*a*), positions x/H = 0.33, 0.66 and 1.00

This model considers the diffusion in a flow of large scale turbulence, where the dispersion of the plume is linearly proportional to the distance from the emission source.

As it can be noted from Eq. 10, the minimum dilution, considering a linear plume dispersion, varies with the square of the distance and depends on the relation between momentum M and empirical constants. Similar expressions were used, for example, for control and prevision of gas emissions (Saathoff *et al.*1998).

In Fig. 18, experimental values and the minimum dilution curves are presented for M = 0.245, conditions (*a*) and (*b*), and M = 0.414, condition (*c*). The experimental values were always larger than the minimum dilution. Configuration I, which presents the closest values to D_{min}, exhibits a definite trend. For conditions (*e*) and (*f*), the dilution increases in a location closer to the beginning of the plume.

These conditions present a smaller momentum ratio, see Table 1. At location $x/H = 1.80$, for condition (*h*), the dilution decreases as a consequence of the large momentum ratio. This behavior is consistent with the influence of *M* on the curves of minimum dilution.

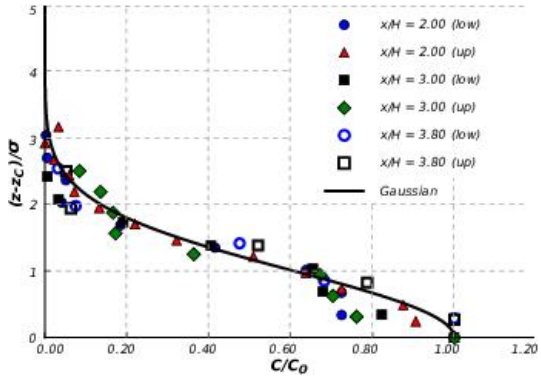

Fig. 15 Gaussian profile and mean concentration experimental values, configuration *I*, condition (*a*), positions $x/H = 2.00$, 3.00 and 3.80

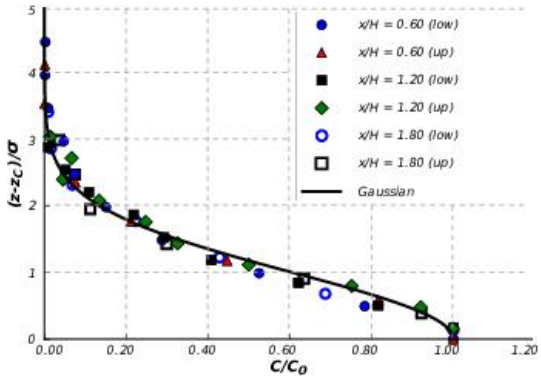

Fig. 16 Gaussian profile and mean concentration experimental values, configuration *I*, condition (*b*), positions $x/H = 0.60$, 1.20 and 1.80

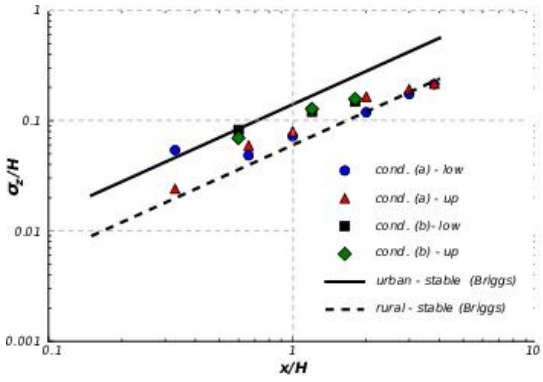

Fig. 17 Comparison of the experimental values of the plume vertical dispersion σ_z, configuration *I*, versus expression of Briggs for neutrally stable atmospheric conditions

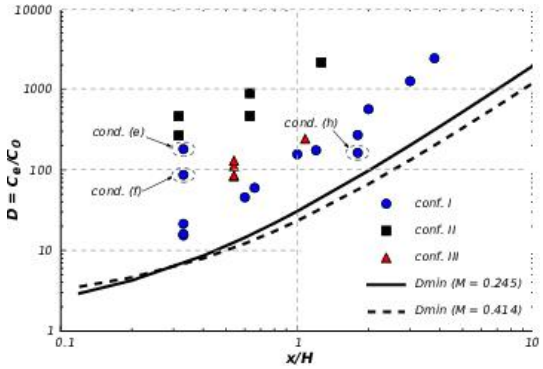

Fig. 18 Experimental values of dilution and curves of minimum dilution

3.6 Intermittency

The statistical analysis of concentration fluctuations is a very important issue for a better understanding of the physical phenomenon and for developing mathematical models. Also, it allows estimating maximum concentration levels even when mean concentration values are relatively low. In this respect, the estimation of the intermittency factor *I*, usually defined as the fraction of non-zero concentration readings, is essential (Wilson *et al.* 1985).

Concentration measurements at the downstream plane $x/H = 0.33$ of the emission source were analyzed for configuration *I*, condition (*a*). Furthermore, three different positions in the plume were studied. Figs. 19-21 show the concentration fluctuation time trace near the plume upper edge ($z/H = 1.26$), near the plume lower edge ($z/H = 0.96$) and near the plume centre ($z/H = 1.12$), respectively. Included on these figures are the mean concentration *C* and $C + 3\sigma_c$ (Mylne and Mason 1991).

For the position near the upper edge of the plume, Fig. 19, it can be noted that the maximum observed concentrations exceeded in approximately three times the value $C + 3\sigma_c$, evidencing a highly skewed concentration probability density function (PDF). The measurements at the lower edge of the plume, Fig. 20, exhibits the same behavior but less skewed. Although these traces are rather similar, this solely analysis is not enough to differentiate statistical characteristics, as will be shown in the remain of this section.

Quite different situation is presented in Fig. 21, corresponding at, approximately, the central position of the plume. Here the intermittency factor is higher and the maximum concentration values are of the order of $C + 3\sigma_c$.

The comparison of the shape of three different probability distribution models to the observed concentration data were also performed. To this end, the cumulative distribution function (CDF), $F(c)$, and exceedance probability distribution, $1 - F(c)$, of the concentrations were computed from the plume concentration data and compared to the clipped normal, exponential and log-normal exceedance probability distribution models (Lewellen and Sykes 1986, Hanna 1984, Csanady 1973, Nakayama and Nagai 2011). The distributions were plotted in the Weibull format (Cheung and Melbourne 2000).

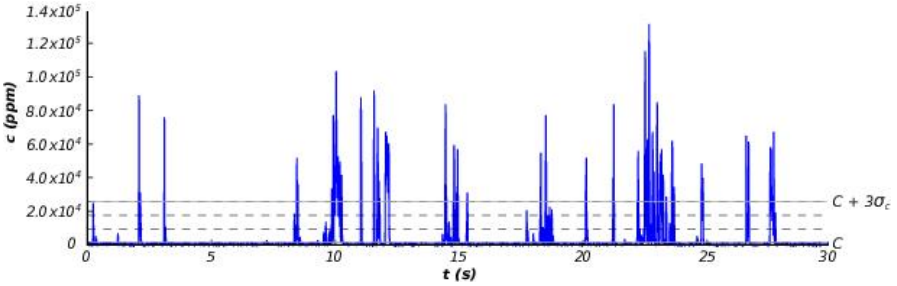

Fig. 19 Concentration fluctuation time tracer at plume upper edge (*z/H* = 1.26). Configuration *I*, condition (*a*)

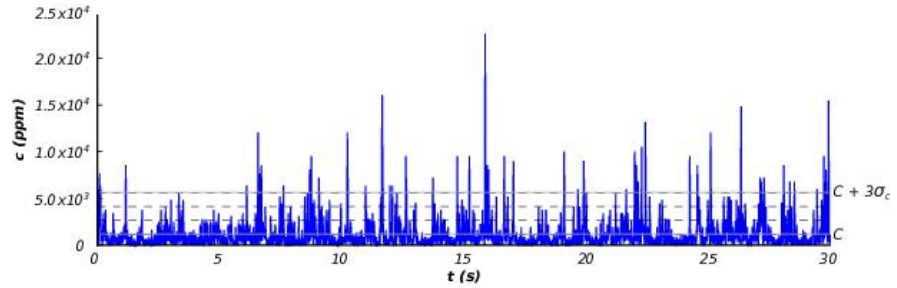

Fig. 20 Concentration fluctuation time tracer at plume lower edge (*z/H* = 0.96). Configuration *III*, condition (*b*)

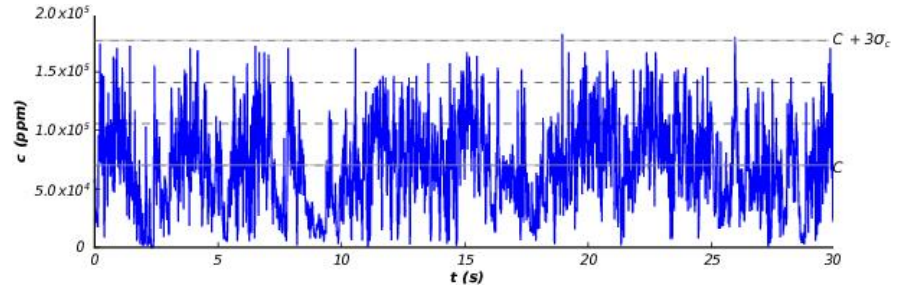

Fig. 21 Concentration fluctuation time tracer at plume centre (*z/H* = 1.12). Configuration *I*, condition (*a*)

In Fig. 22(a) the CDF of the concentration fluctuations at a distance *x/H* = 0.33 from the emission source are plotted. It can be seen that near the plume centre (*z/H* = 1.12), the slope of the probability distribution in Weibull format is steeper. A decrease of this slope indicates an increasing intermittency across the plume (Cheung and Melbourne 2000), with a lower value of *I* at the plume upper edge (*z/H* = 1.26) than at the plume lower edge (*z/H* = 0.96$). It is possible to explain this behavior as a product of different buoyancy effects upwards and downwards of the plume centreline.

The probability density function of concentration data may take several different probability distribution models, depending on the region of the plume being measured. According to Cheung and Melbourne 2000), the exponential distribution fits better in meandering plume concentrations near emission sources. The exponential CDF takes the form (Hanna 1984)

$$F(c) = 1 - I^* \exp\left(-I^* \frac{c}{C}\right) \tag{12}$$

being I^* expressed as

$$I^* = 2/\left[(\sigma_c / C)^2 + 1\right] \tag{13}$$

where C and σ_c include all the zero concentration values.

The concentration distribution near the plume centreline is well approximated by the Gaussian form. Lewellen and Sykes (1986) found that in presence of any non-realizable negative concentration tail, the distribution takes a Gaussian form with a delta function at zero concentration, representing the intermittency of the local concentration. This distribution is known as clipped normal, whose CDF is of the form

$$F(c) = \frac{1}{2}\left[1 - \mathrm{erf}\left(\frac{c - C}{\sqrt{2}\sigma_c}\right)\right] \tag{14}$$

where erf is the error function.

The last distribution used for comparison in this work is the log-normal distribution (Csanady 1973). The CDF of this distribution is

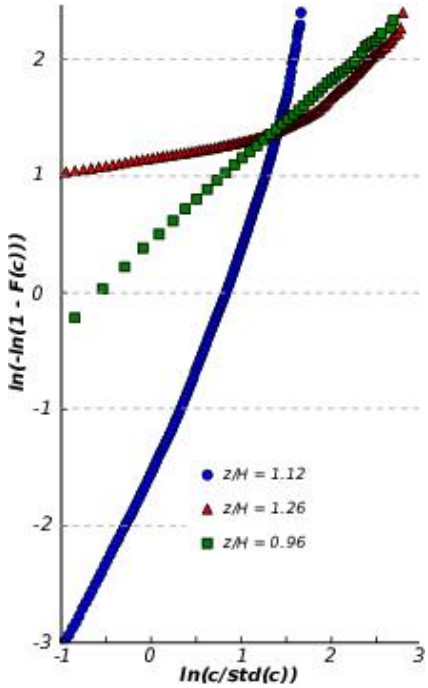

(a) Exceedance probability distribution of concentration measured at z/H = 1.26, 1.12 and 0.96

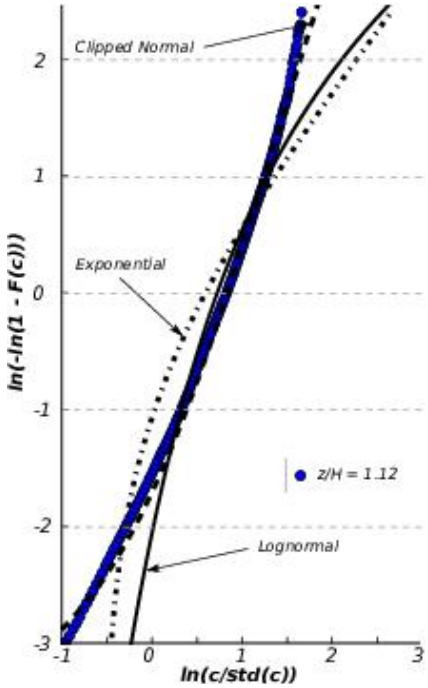

(b) Exceedance probability distribution of concentration measured at plume center (z/H = 1.12) compared against the log-normal, exponential and clipped normal distributions

Fig. 22 Exceedance probability distribution against the number of standard deviation of concentration exceedance. Configuration *I*, condition (*a*)

$$F(c) = \frac{1}{2}\left[1 + \mathrm{erf}\left(\frac{\ln(c/C_m)}{\sqrt{2}\sigma_{lc}}\right)\right] \tag{15}$$

where C_m is the median concentration

$$C_m = \frac{C}{\sqrt{(\sigma_c/C)^2 + 1}} \tag{16}$$

and σ_{lc} is the logarithmic standard deviation

$$\sigma_{lc} = \sqrt{\ln[(\sigma_c/C)^2 + 1]}. \tag{17}$$

Fig. 22(b) shows a comparison between exceedance probability distribution of concentration data at z/H = 1.12 and the theoretical models. In order to evaluate the theoretical models, statistics of the measured concentrations were used. From this figure it is possible to observe a good approximation to the clipped normal distribution while the log-normal distribution fits approximately the data in the logarithmical normalized concentration range of 0.25-1.25.

At z/H = 1.26, Fig. 23(a), it can be seen that probability distribution of the concentration data is consistent with the exponential distribution in almost all the concentration variation range. The concentration CDF at z/H = 0.96, Fig. 23(b), conform more closely to the log-normal distribution even though there is a mismatch in the tails of the distribution.

Findings from these analyses revealed the different behaviors of the dispersion mechanisms in a cross-sectional plane inside the plume. The distributions at the upper edge of the plume was shown to change from an exponential form towards a clipped normal form near the lower edge.

5. Conclusions

In this work, the dispersion process of an emission plume is studied experimentally through field concentration measurements using a reduced model in a wind tunnel. Three configurations with distinctive features in terms of the dispersion process were tested. Statistical characteristics of the concentration measurements were extracted and analyzed.

A previous experimental analysis of the incident wind characteristics has shown fluctuations of the velocity dispersion when measurements at very low flow velocity were performed. The general behavior of the profiles of concentration coefficient and intensity of concentration fluctuations were quantified and described for several distances from the emission source and under different conditions. It is worth noting that a major asymmetry between the upper and lower regions was found, as a consequence of the buoyancy generated by the emission of a light gas as the helium. Theoretical models for the analysis of the standard deviation of the fluctuations do not consider this asymmetry.

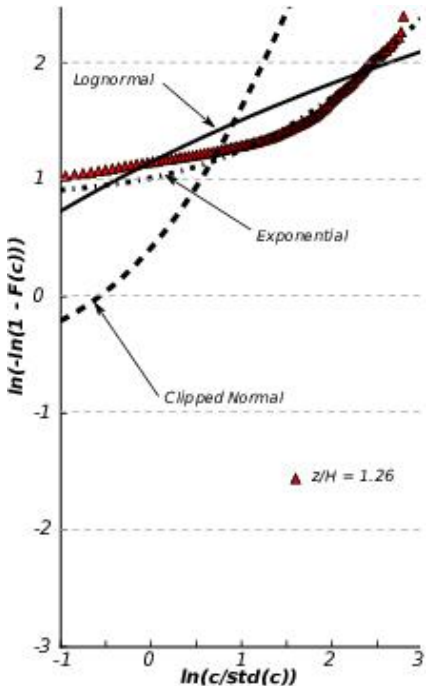

(a) Concentration measured at plume upper edge (z/H = 1.26)

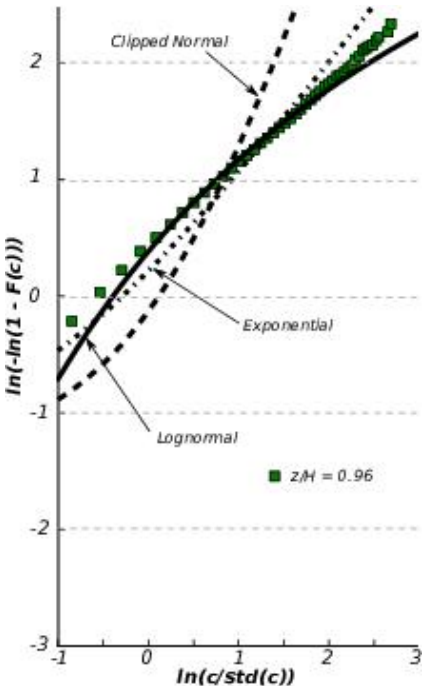

(b) Concentration measured at plume lower edge (z/H = 0.96)

Fig. 23 Exceedance probability distribution against the number of standard deviation of concentration exceedance. Measured concentrations and log-normal, exponential and clipped normal distributions. Configuration *I*, condition (*a*).

The plume emission and buoyancy conditions have influence in the process, but this influence is relevant only in the configurations corresponding to the single building model near the emission source.

The distributions of the mean concentrations are, in general, similar to Gaussian configurations, except for the case in which the prismatic building model is located windward from the emission source. Major irregularities in the concentration fluctuation intensity profiles were observed for conditions (*a*), (*c*) and (*d*), measured with low wind velocity conditions. Nevertheless, the measurements obtained in this work are in good agreement with the results of theoretical models proposed in previous works.

For the case of an isolated source emission, the intermittency at different dispersion plume regions near the emission source has been analyzed using cumulative probability distributions. The slope of the plot in Weibull form was used to determine the intermittency of the concentration. Near the emission source, the process is highly intermittent at the upper edge extremity of the plume decreasing to the plume centreline. It is worth noting that different statistical descriptions of the concentration fluctuation data were observed by modifying the measurement position inside the plume.

Based on this analysis it is possible to conclude that the experimental arrangement outlined in this work is suitable for evaluating problems of turbulent diffusion. Further research will focus on other urban environment configurations and comparisons with computational simulations.

Acknowledgments

The authors are grateful to CAPES, Brazil, for the financial support conceded. This research was partially funded by Conselho Nacional de Desenvolvimento Científico e Tecnológico (CNPq, Brasil), Secretaríaa General de Ciencia y Técnica de la Universidad Nacional del Nordeste (SGCYT-UNNE, Argentina), Consejo Nacional de Investigaciones Científicas y Técnicas (CONICET, Argentina) and Secretaría de Ciencia y Tecnología de la Universidad Tecnológica Nacional Facultad Regional Resistencia (UTN-FRRe, Argentina, Grant PID 4061TC (2016)). Also, the authors would like to acknowledge the financial support from the Agencia Nacional de Promoción Científica y Tecnológica (ANPCyT, Argentina, Grant PICT 2015 IB CONICET 2739).

References

Baechlin, W., Theurer, W. and Plate, E.J. (1992), "Dispersion of gases released near the ground in built up areas: Experimental results compared to simple numerical modelling", *J. Wind Eng. Ind. Aerod.*, **44**(1-3), 2721-2732.

Blessmann, J. (1982), "The boundary layer wind tunnel of the UFRGS", *J. Wind Eng. Ind. Aerod.*, **10**(2) 231-248.

Camano Schettini, E.B. (1996), "Etude expérimentale des jets coaxiaux avec différences de densité", Thèse de Docteur, Institut National Polytechnique de Grenoble, France.

Cermak, J.E. and Takeda, K. (1985), "Physical modeling of urban air-pollutant transport", *J. Wind Eng. Ind. Aerod.*, **21**, 51-67.

Cheung, J.C.K. and Melbourne, W.H. (2000), "Probability distribution of dispersion from a model plume in turbulent

wind", *J. Wind Eng. Ind. Aerod.*, **87**(2-3), 271-285.
Chui, E. and Wilson, D. (1988), "Effect of varing wind direction on exhaust gas dilution", *J. Wind Eng. Ind. Aerod.*, **31**(1), 87-104.
Csanady, G.T. (1973), *Turbulent Diffusion in the Environment*, D. Reidel Publishing Co., Dordrecht, Holland, 222–248.
Fothergill, C.E., Roberts, P.T. and Packwood, A.R. (2002), "Flow and dispersion around storage tanks. A comparison between numerical and wind tunnel simulations", *Wind Struct.*, **5**(2-4), 89-100.
Gousseau, P., Blocken, B. and van Heijst, G.J.F. (2012), "Large-Eddy Simulation of pollutant dispersion around a cubical building: Analysis of the turbulent mass transport mechanism by unsteady concentration and velocity statistics", *Environ. Pollution*, **167**, 47–57.
Gousseau, P., Blocken, B., Stathopoulos, T. and van Heijst, G.J.F. (2011), "CFD simulation of near-field pollutant dispersion on a high-resolution grid: A case study by LES and RANS for a building group in downtown Montreal", *Atmos. Environ.*, **45**(2), 428-438.
Hanna, S.R. (1984), "The exponential probability density function and concentration fluctuations in smoke plumes", *Bound.-Lay. Meteorol.*, **29**(4), 361-375.
Harion, J.L., Favre-Marinet, M. and Camano, B. (1996), "An improved method for measuring velocity and concentration by thermo-anemometry in turbulent helium-air mixtures", *Exp. Fluids*, **22**(2).
Isyumov, N. and Tanaka, H. (1980), "Wind tunnel modelling of stack gas dispersion - difficulties and approximations", *Proceedings of the 5th International Conference on Wind Engineering*, Fort Collins, Colorado, USA.
Kim, J.J., Song, H.J. and Baik, J.J. (2006), "Modeling flow and scalar dispersion around Cheomseongdae", *Wind Struct.*, **9**(4), 315-330.
Lateb, M., Masson, C., Stathopoulos, T. and Bèdard, C. (2011), "Effect of stack height and exhaust velocity on pollutant dispersion in the wake of a building", *Atmos. Environ.*, **45**(29), 5150-5163.
Lewellen, W.S. and Sykes, R.I. (1986), "Analysis of concentration fluctuations from lidar observations of atmospheric plumes", *J. Climate Appl. Meteorol.*, **25**(8), 1145-1154.
Liu, G., Xuan, J. and Park, S.U. (2003), "A new method to calculate wind profile parameters of the wind tunnel boundary layer", *J. Wind Eng. Ind. Aerod.*, **91**(9), 1155-1162.
Loredo-Souza, A.M., Camaño Schettini, E.B. and Paluch, M.J. (2004), "Simulação da camada limite atmosférica em túnel de vento", in *Turbulência*, Vol. 4, edited by Möller, S.V., and Silvestrini, J., Associação Brasileira de Engenharia e Ciências Mecânicas, ABCM, Brazil.
Mylne, K.R. and Mason, P.J. (1991), "Concentration fluctuation measurements in a dispersing plume at a range of up to 1000 m", *Q. J. Roy. Meteor. Soc.*, **117**(497), 177-206.
Nakayama, H. and Nagai, H. (2011), "Development of local-Scale high-resolution atmospheric dispersion model using large-eddy simulation part 2: Turbulent flow and plume dispersion around a cubical building", *J. Nuclear Sci. Technol.*, **48**(3), 374-383.
Perry, S.G., Heist, D.K., Brouwer, L.H., Monbureau, E.M. and Brixey, L.A. (2016), "Characterization of pollutant dispersion near elongated buildings based on wind tunnel simulations", *Atmos. Res.*, **142**, 286-295.
Quinn, A.D., Wilson, M., Reynolds, A.M., Couling, S.B. and Hoxey, R.P. (2001), "Modelling the dispersion of a tracer gas in the wake of an isolated low-rise building", *Wind Struct.*, **4**(1), 31-44.
Robins, A. (2003), "Wind tunnel dispersion modeling some recent and not so recent achievements", *J. Wind Eng. Ind. Aerod.*, **91**, 1777-1790.
Robins, A., Castro, I., Hayden, P., Steggel, N., Contini, D. and Heist, D. (2001), "A wind tunnel study of dense gas dispersion in a neutral boundary layer over a rough surface", *Atmos. Environ.*, **35**(13), 2243-2252.
Saathoff, P., Stathopoulos, T. and Wu, H. (1998), "The influence of freestream turbulence on nearfield dilution of exhaust from building vents", *J. Wind Eng. Ind. Aerod.*, **77-78**, 741-752.
Thompson, R.S. (1993), "Building amplification factors for sources near buildings: A wind-tunnel study", *Atmos. Environ.*, **27** 15, 2313-2325.
Vervecken, L., Camps, J. and Meyers, J. (2013), "Accounting for wind-direction fluctuations in Reynolds-averaged simulation of near-range atmospheric dispersion", *Atmos. Environ.*, **72**, 142-150.
White, B.R. and Stein, W. (1990), "Wind-Tunnel studies of variable stack heights for a low-profile building", *J. Wind Eng. Ind. Aerod.*, **36**(1), 675-687.
Wilson, D.J., Robins, A.G. and Fackrell, J.E. (1985), "Intermittency and conditionally-averaged concentration fluctuation statistics in plumes", *Atmos. Environ.*, **19**(7), 1053-1064.
Yassin, M.F., Katob, S., Ookab, R., Takahashib, T. and Kounob, R. (2005), "Field and wind-tunnel study of pollutant dispersion in a built-up area under various meteorological conditions", *J. Wind Eng. Ind. Aerod.*, **93**, 361-382.
Yu, H. and Thè, J. (2016), "Validation and optimization of SST k-! turbulence model for pollutant dispersion within a building array", *Atmos. Environ.*, **145**, 225-238.
Zannetti, P. (1990), *Air Pollution Modeling - Theories, Computational Methods and Available Software*, Springer US.

AD